Electronic Supplementary Information

Efficient vacuum deposited p-i-n and n-i-p perovskite solar cells employing doped charge transport layers

Cristina Momblona[1,†], Lidón Gil-Escrig[1,†], Enrico Bandiello[1], Eline M. Hutter[2], Michele Sessolo[1], Kay Lederer[3], Jan Blochwitz-Nimoth[3]* and Henk J. Bolink[1]*

[1]Instituto de Ciencia Molecular, Universidad de Valencia, C/ Catedrático J. Beltrán 2, 46980 Paterna (Valencia), Spain

[2]Department of Chemical Engineering, Delft University of Technology, Van der Maasweg 9, 2629 HZ Delft, the Netherlands

[3]NOVALED GmbH, Tatzberg 49, 01307 Dresden, Germany

*Corresponding author. E-mail: jan.bn@novaled.com and henk.bolink@uv.es

Experimental

Materials. Photolithographically patterned ITO coated glass substrates were purchased from Naranjo Substrates (www.naranjosubstrates.com). 2,2'-(Perfluoronaphthalene-2,6-diylidene) dimalononitrile (F6-TCNNQ), N4,N4,N4",N4"-tetra([1,1'-biphenyl]-4-yl)-[1,1':4',1"-terphenyl]-4,4"-diamine (TaTm) and N1,N4-bis(tri-p-tolylphosphoranylidene)benzene-1,4-diamine (PhIm) were provided from Novaled GmbH. Fullerene (C_{60}) was purchased from sigma Aldrich. PbI_2 was purchased from Tokyo Chemical Industry CO (TCI), and CH_3NH_3I (MAI) from Lumtec.

Device preparation. ITO-coated glass substrates were subsequently cleaned with soap, water and isopropanol in an ultrasonic bath, followed by UV-ozone treatment. They were transferred to a vacuum chamber integrated into a nitrogen-filled glovebox (MBraun, H_2O and O_2 < 0.1 ppm) and evacuated to a pressure of $1 \cdot 10^{-6}$ mbar. The vacuum chamber uses a turbomolecular pump (Pfeiffer TMH 261P, DN 100 ISO-K, 3P) coupled to a scroll pump. This system is very robust and has been used continuously for over two years. The blades of the turbomolecular pump are cleaned roughly every year after which they continue to operate. The vacuum chamber is equipped with six temperature controlled evaporation sources (Creaphys) fitted with ceramic crucibles. The sources were directed upwards with an angle of approximately 90° with respect to the bottom of the evaporator. The substrate holder to evaporation sources distance is approximately 20 cm. Three quartz crystal microbalance (QCM) sensors are used, two monitoring the deposition rate of each evaporation source and a third one close to the substrate holder monitoring the total deposition rate. For thickness calibration, we first individually sublimed the charge transport materials and their dopants (TaTm and F_6-TCNNQ, C_{60} and PhIm). A calibration factor was obtained by comparing the thickness inferred from the QCM

sensors with that measured with a mechanical profilometer (Ambios XP1). Then these materials were co-sublimed at temperatures ranging from 135-160 ºC for the dopants to 250 ºC for the pure charge transport molecules, and the evaporation rate was controlled by separate QCM sensors and adjusted to obtain the desired doping concentration. In general, the deposition rate for TaTm and C_{60} was kept constant at 0.8 Å s^{-1} while varying the deposition rate of the dopants during co-deposition. Pure TaTm and C_{60} layers were deposited at a rate of 0.5 Å s^{-1}. For the *p-i-n* configuration, 40 nm of the p-doped hole-transport layer (p-HTL, TaTm:F_6-TCNNQ) capped with 10 nm of the pure TaTm were deposited. Once completed this deposition, the chamber was vented with dry N_2 to replace the p-HTL crucibles with those containing the starting materials for the perovskite deposition, PbI_2 and CH_3NH_3I. The vacuum chamber was evacuated again to a pressure of 10^{-6} mbar, and the perovskite films were then obtained by co-deposition of the two precursors. The calibration of the deposition rate for the CH_3NH_3I was found to be difficult due to non-uniform layers and the soft nature of the material which impeded accurate thickness measurements. Hence, the source temperature of the CH_3NH_3I was kept constant at 70 ºC and the CH_3NH_3I:PbI_2 ratio was controlled off line using grazing incident x-ray diffraction by adjusting the PbI_2 deposition temperature. The optimum deposition temperatures were found to be 250 ºC for the PbI_2 and 70 ºC for the CH_3NH_3I. After deposition of a 500 nm thick perovskite film, the chamber was vented and the crucibles replaced with those containing C_{60} and PhIm, and evacuated again to a pressure of 10^{-6} mbar. The devices were completed depositing a film of pure C_{60} and one of the n-ETL (C_{60}:PhIm), with thicknesses of 10 and 40 nm, respectively. This process of exchanging crucibles was done to evaluate the effect of changes in the organic layer composition for an identical perovskite layer. In one evaporation run we can prepare 5 substrates (3 by 3 cm) each containing 4 cells. Generally, one substrate was reserved for a reference

configuration allowing to evaluate 4 variations in the transport layers per perovskite evaporation. It is also possible to prepare the complete stack without breaking vacuum as we have 6 sources available. Finally the substrates were transferred to a second vacuum chamber where the metal top contact (100 nm thick) was deposited. For *n-i-p* devices, the exact same procedure as described before was used in the inverted order.

Characterization. Grazing incident X-ray diffraction (GIXRD) pattern were collected at room temperature on an Empyrean PANanalytical powder diffractometer using the Cu Kα1 radiation. Typically, three consecutive measurements were collected and averaged into single spectra. The surface morphology of the thin films was analyzed using atomic force microscopy (AFM, Multimode SPM, Veeco, USA). Scanning Electron Microscopy (SEM) images were performed on a Hitachi S-4800 microscope operating at an accelerating voltage of 2 kV over Platinum - metallized samples. Absorption spectra were collected using a fiber optics based Avantes Avaspec2048 Spectrometer. Characterization of the solar cells was performed as follows. The external quantum efficiency (EQE) was estimated using the cell response at different wavelength (measured with a white light halogen lamp in combination with band-pass filters), where the solar spectrum mismatch is corrected using a calibrated Silicon reference cell (MiniSun simulator by ECN, the Netherlands). The current density-voltage (J-V) characteristics were obtained using a Keithley 2400 source measure unit and under white light illumination, and the short circuit current density was corrected taking into account the device EQE. The electrical characterization was validated using a solar simulator by Abet Technologies (model 10500 with an AM1.5G xenon lamp as the light source). Before each measurement, the exact light intensity was determined using a calibrated Si reference diode equipped with an infrared cut-off filter (KG-3, Schott). Importantly, no difference in the J-V characteristics was observed as a function

of evaluation method. The J-V curves were recorded between -0.2 and 1.2 V with 0.01V steps, integrating the signal for 20 ms after a 10 ms delay. This corresponds to a speed of about 0.3 V s^{-1}. Two different devices layout has been used to test the solar cells configurations, one with four equal areas (0.0653 cm^2, defined as the overlap between the ITO and the top metal contact) and measured through a shadow masks with 0.01 cm^2 aperture, and a second with increasing areas (0.0897 cm^2, 0.1522 cm^2, 0.3541 cm^2 and 0.9524 cm^2) which was characterized using a shadow mask with aperture areas of 0.0484 cm^2, 0.1024 cm^2, 0.2704 cm^2 and 0.8464 cm^2, respectively. For hysteresis study, different scan rates (0.1, 0.5 and 1 Vs^{-1}) were used, biasing the device from -0.2 to 1.2 V with 0.01 V steps and vice versa. Light intensity dependence measurements were done by placing 0.1, 1, 10, 20, 50% neutral density filters (LOT-QuantumDesign GmbH) between the light source and the device.

Photoconductance measurements. Thin films on quartz substrates were placed in a sealed resonance cavity inside an N_2-filled glovebox. The time resolved microwave conductivity (TRMC) technique was used to measure the change in microwave (8-9 GHz) power after pulsed excitation (repetition rate 10 Hz) of the $MAPbI_3$ films at 650 nm. The photoexcitation-induced change in microwave power is related to the change in conductance ΔG by a sensitivity factor K:

$$\frac{\Delta P(t)}{P} = -K\Delta G(t)$$

The rise of ΔG is limited by the width of the laser pulse (3.5 ns FWHM) and the response time of our microwave system (18 ns). The slow repetition rate of the laser of 10 Hz ensures full relaxation of all photo-induced charges to the ground state before the next laser pulse hits the sample. The product of yield Φ and mobility ($\mu_e + \mu_h$) is calculated from the maximum change in photo-conductance ΔG_{max} by:

$$\varphi\Sigma\mu = \frac{\Delta G_{max}}{I_0 \beta e F_A}$$

Here, I_0 is the number of photons per unit area per pulse, β is the ratio of the inner dimensions of the microwave cell, e the elementary charge and F_A the fraction of light absorbed by the sample at the excitation wavelength (650 nm). Before and during the photoconductance measurements, the samples were not exposed to moisture and air to prevent degradation. The charge carrier diffusion length L_D was calculate by estimating the mobility μ and the half lifetime t, using the relation:

$$L_D = \sqrt{D\tau}$$

Where $D = \sum \mu k_B T/e$, with k_B the Boltzmann constant and T the temperature.

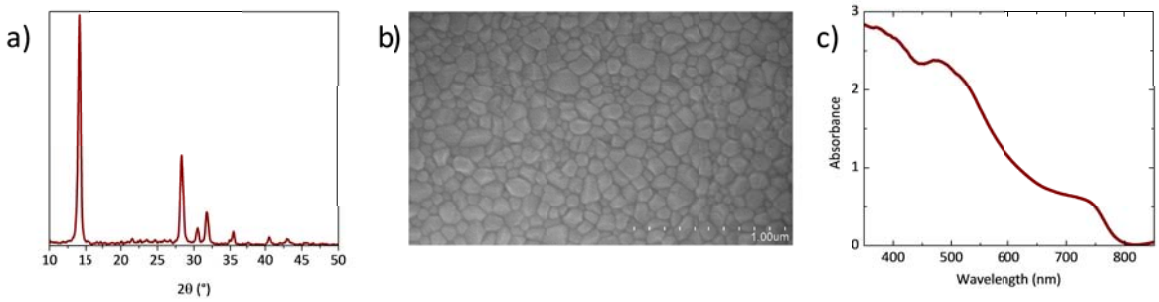

Fig. S1 (a) GIXRD pattern, (b) surface SEM picture and (c) optical absorbance of the vacuum deposited $MAPbI_3$ thin films used for *p-i-n* and *n-i-p* cells preparation.

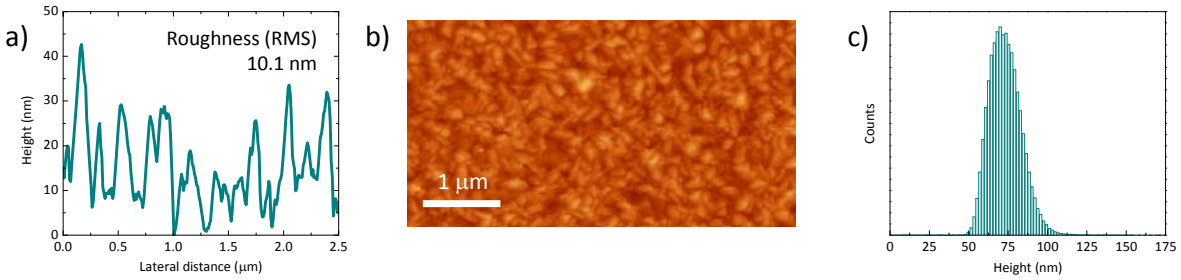

Fig. S2 Atomic force microscopy (AFM) characterization of the vacuum deposited $MAPbI_3$ thin films used for *p-i-n* and *n-i-p* cells preparation: (a) Surface profile, (b) topography and (c) roughness analysis

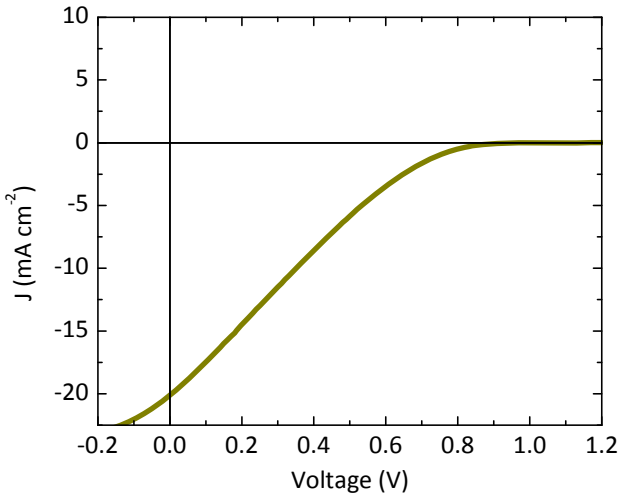

Fig. S3 J-V scan for a *p-i-n* device with the structure ITO/TaTm (40 nm)/$MAPbI_3$ (500 nm)/ C_{60} (40 nm)/Ag.

Table S1 Photovoltaic parameters for the main solar cells architecture studied. The effect of the selective removal of the intrinsic charge transport layers is highlighted.

	Device structure	V_{oc} (mV)	J_{sc} (mA cm^{-2})	FF (%)	PCE (%)
	TaTm/$MAPbI_3$/C_{60}	1041	20.12	16.8	3.5
	p-HTL/TaTm/$MAPbI_3$/C_{60}/n-ETL	1082	20.02	73.1	15.8
p-i-n	**p-HTL/**$MAPbI_3$/C_{60}/n-ETL	**1033**	20.19	73.3	15.3
	p-HTL/TaTm/$MAPbI_3$**/n-ETL**	1032	17.82	**45.0**	8.3
	n-ETL/C_{60}/$MAPbI_3$/TaTm/p-HTL	1115	20.28	79.8	18.0
n-i-p	**n-ETL/**$MAPbI_3$/TaTm/p-HTL	1084	20.45	**68.8**	15.2
	n-ETL/C_{60}/$MAPbI_3$**/p-HTL**	**998**	19.44	**68.7**	13.3

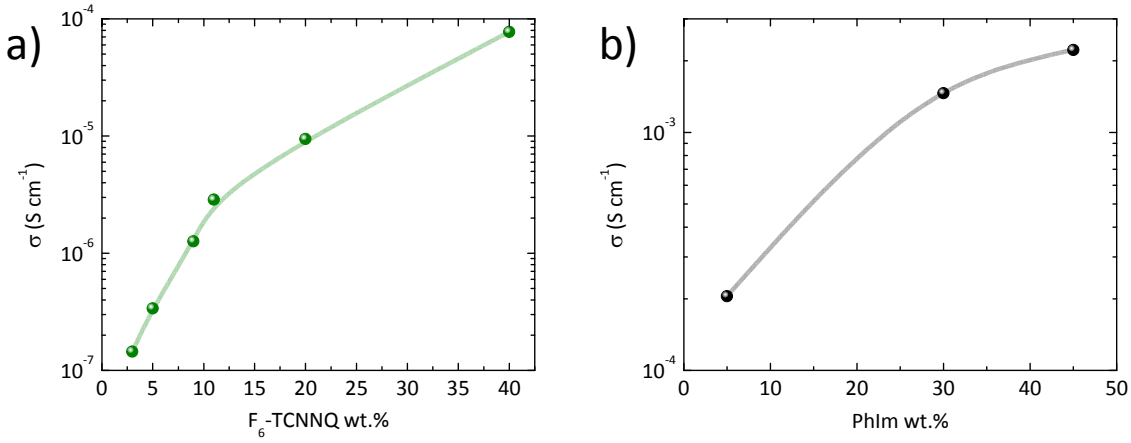

Fig. S4 Conductivity as a function of the dopant concentration for 100 nm thick films of (a) p-HTL (TaTm:F_6-TCNNQ) and (b) n-ETL (C_{60}:PhIm).

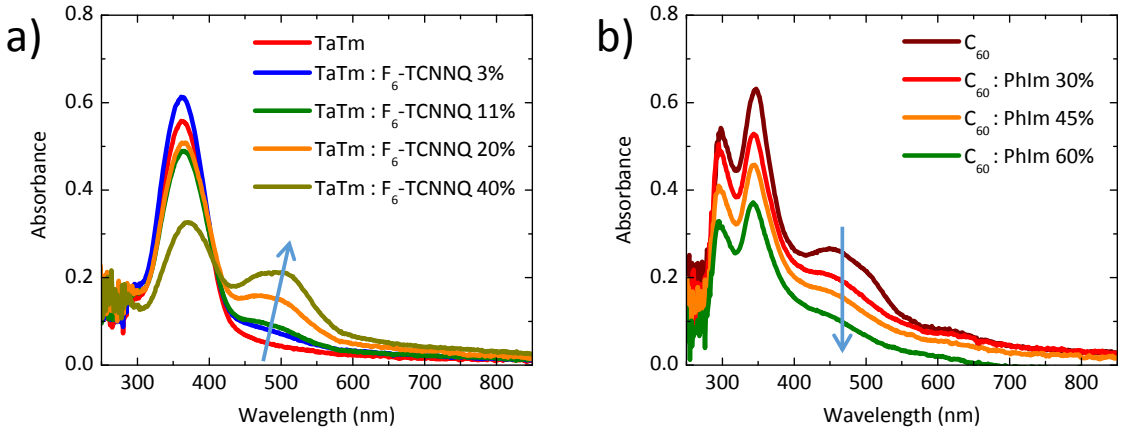

Fig. S5 Optical absorbance as a function of the dopant concentration for 40 nm thick films of (a) p-HTL (TaTm:F_6-TCNNQ) and (b) n-ETL (C_{60}:PhIm).

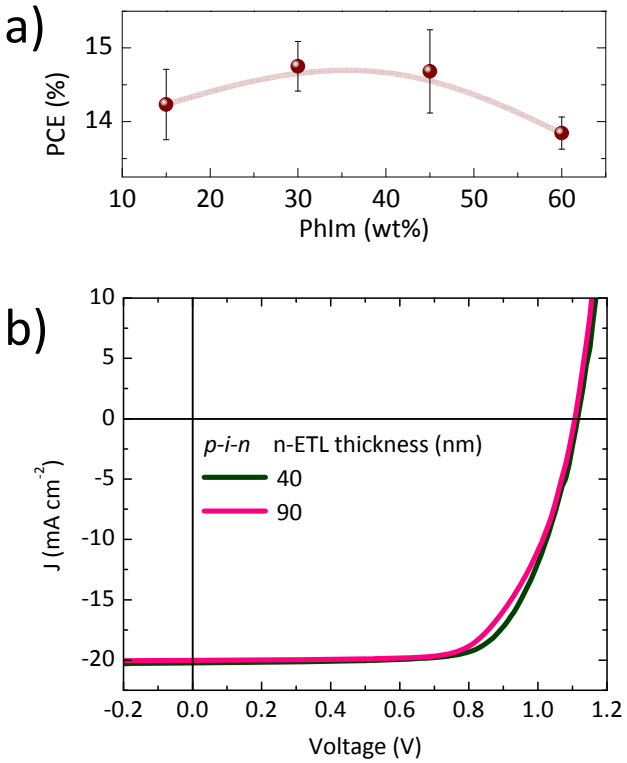

Fig. S6 (a) Trend of the PCE for a series of *p-i-n* cells with increasing concentration of the PhIm dopant in the n-ETL. (b) *J-V* scans for *p-i-n* devices with increasing thickness of the n-ETL (C_{60}:PhIm).

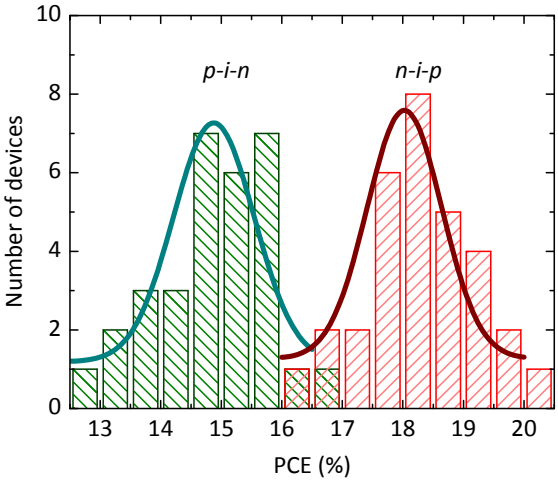

Fig. S7 Statistics of the PCE measured for *p-i-n* (green) and *n-i-p* devices (32 cells for each configuration). Green and red solid lines represent the Gaussian distribution fitting for the PCE.

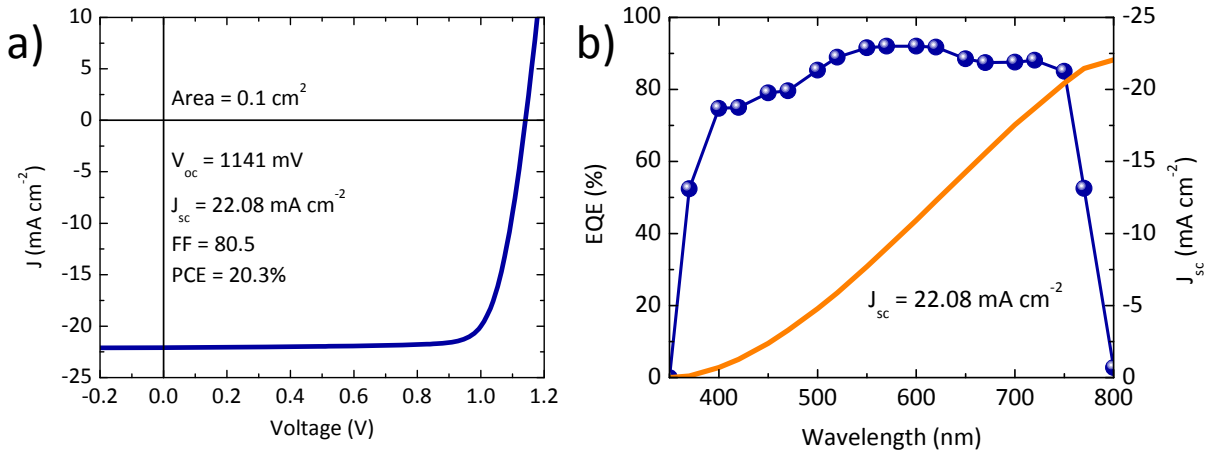

Fig. S8 (a) J-V curves under 100 mW cm^{-2} illumination and (c) EQE spectra (the integrated photocur-rent with the AM1.5G solar spectrum is shown on the right axis) for the top performing *n-i-p* perovskite solar cell.

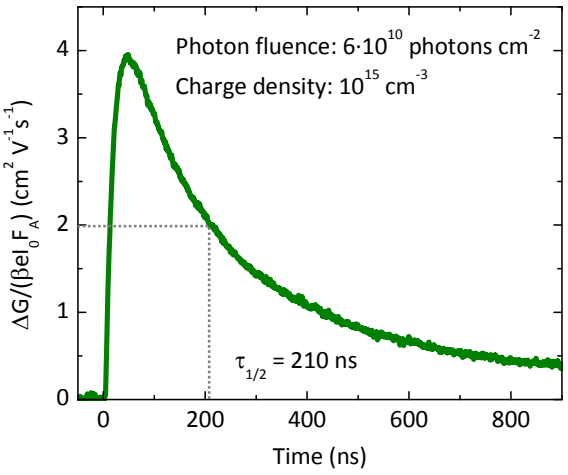

Fig. S9. TRMC trace for a 300 nm thick $MAPbI_3$ film recorded at excitation wavelengths of 650 nm with a fluence of 6·10^{10} photons cm^{-2} per pulse, resulting in a charge density (10^{15} cm^{-3}) corresponding to 1 AM1.5. The extrapolation of the half lifetime t is shown for clarity.

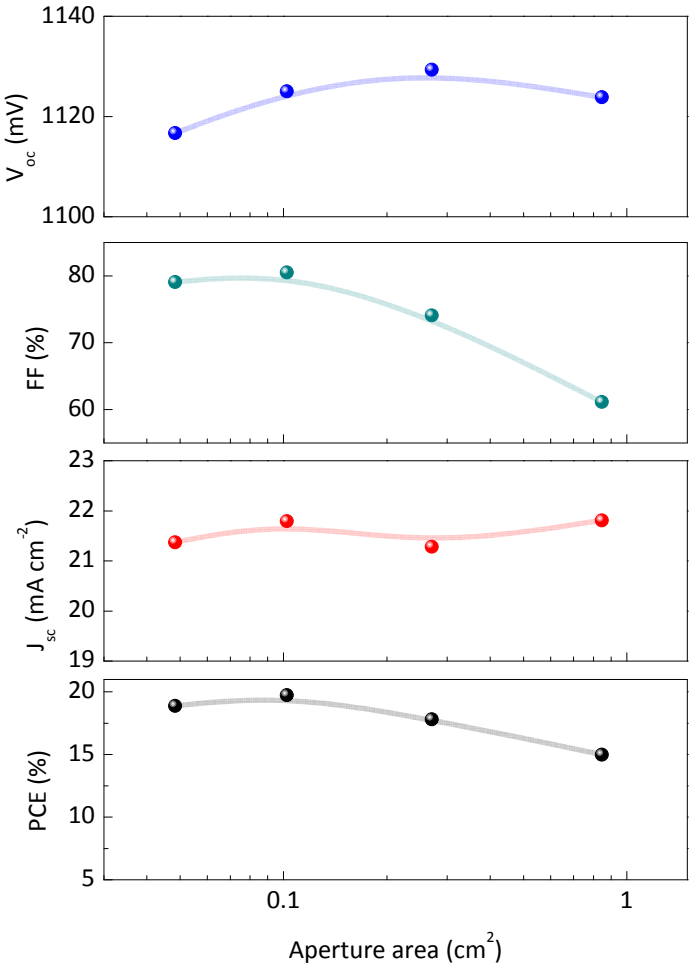

Fig. S10 Photovoltaic parameters extracted from *J-V* and EQE measurements for a series of *n-i-p* devices with increasing area, defined as the shadow mask aperture. Note that the area of the ITO/metal is also increasing proportionally.

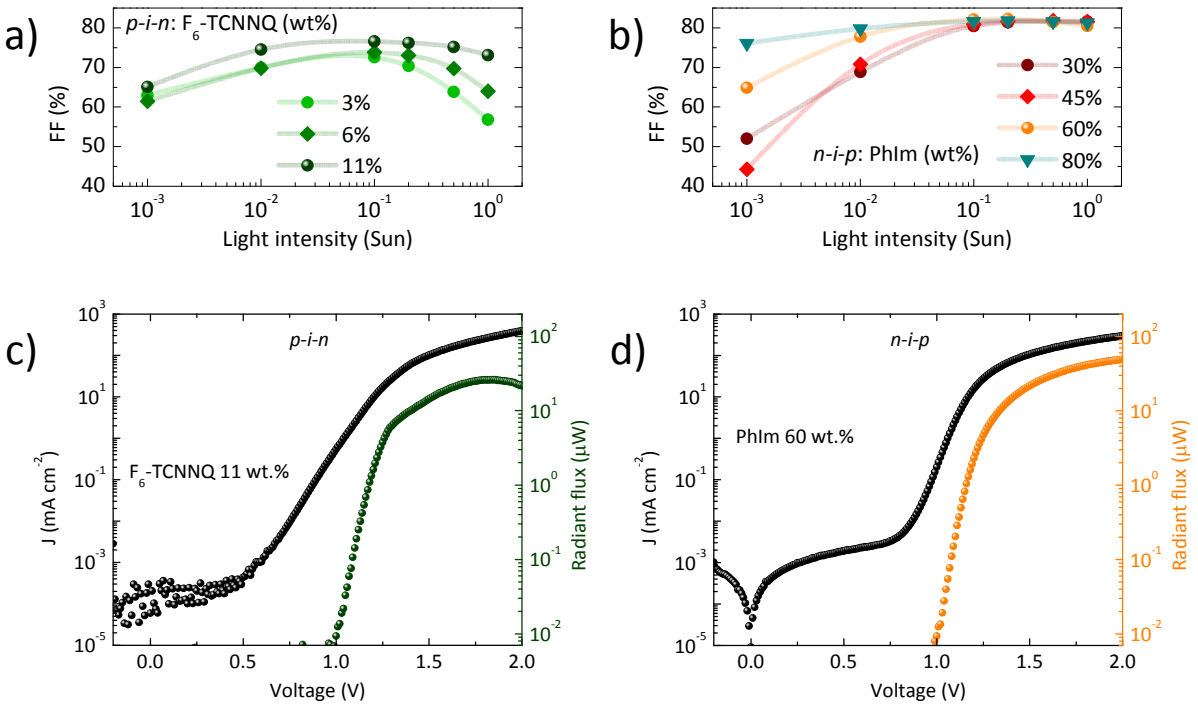

Fig. S11 Light intensity dependence of the measured *FF* for different doping concentration in the charge transport layer at the front contact for (a) *p-i-n* and (b) *n-i-p* cells. *J-V* and electroluminescence characteristics for the 2 reference (c) *p-i-n* and (d) *n-i-p* devices.

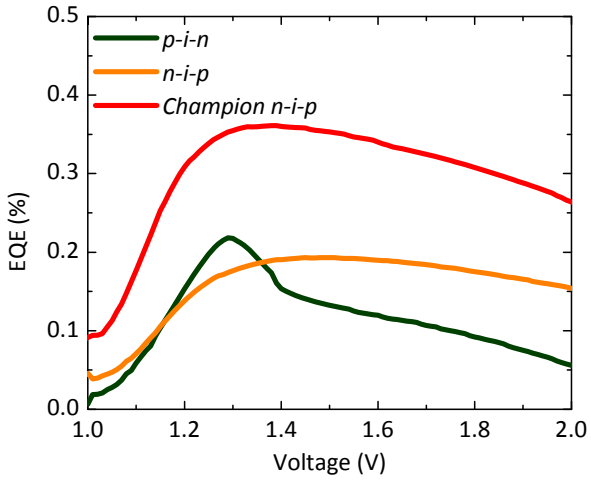

Fig. S12 EQE of electroluminescence for *p-i-n* and *n-i-p* cells. The EQE characteristic for our record PCE *n-i-p* device is shown for comparison.

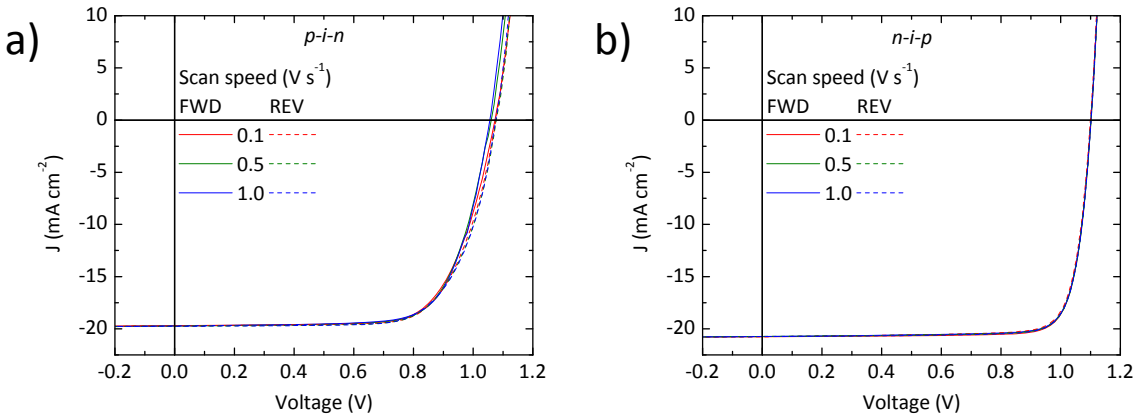

Fig. S13 Characterization of the *J-V* hysteresis of (a) *p-i-n* and (b) *n-i-p* perovskite solar cells, performed by measuring the current as a function of the bias scan direction at different scan speed.

Table S2 Photovoltaic parameters extracted from the *J-V* hysteresis (Fig. S12) for *p-i-n* and *n-i-p* perovskite solar cells, under forward (FWD) and reverse (REV) bias at different scan speed.

	Speed	**0.1 V s^{-1}**		**0.5 V s^{-1}**		**1.0 V s^{-1}**	
	Direction	FWD	REV	FWD	REV	FWD	REV
p-i-n	V_{oc} (mV)	1073	1076	1061	1077	1056	1075
	J_{sc} (mA cm^{-2})	19.65	19.64	19.65	19.65	19.63	19.65
	FF (%)	71.0	71.4	72.3	71.1	72.7	71.0
	PCE (%)	15.0	15.1	15.1	15.0	15.1	15.0
n-i-p	V_{oc} (mV)	1101	1100	1102	1101	1101	1102
	J_{sc} (mA cm^{-2})	20.73	20.73	20.73	20.73	20.73	20.73
	FF (%)	83.0	82.2	82.9	82.7	82.7	82.8
	PCE (%)	19.0	18.7	18.9	18.9	18.9	18.9

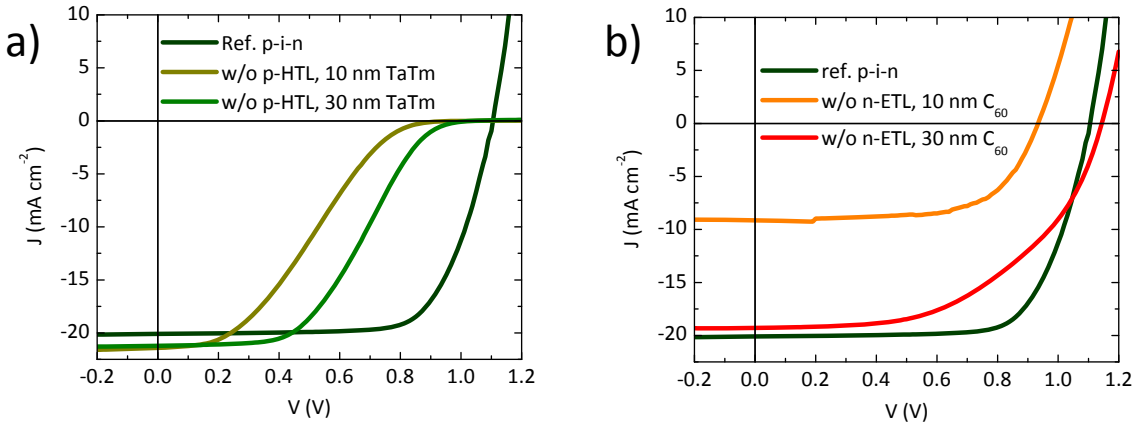

Fig. S14 *J-V* characteristics of *p-i-n* perovskite devices without the (a) p-HTL or the (b) n-ETL, for different thicknesses of the intrinsic TaTm and C_{60} transport layer, respectively.

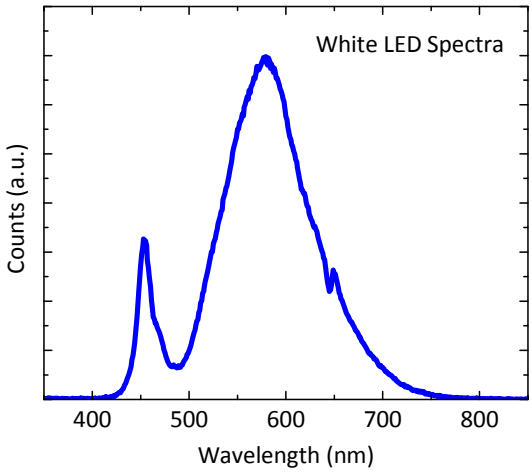

Fig. S15 Optical emission spectra of the white LED used to illuminate the solar cells during lifetime measurements.

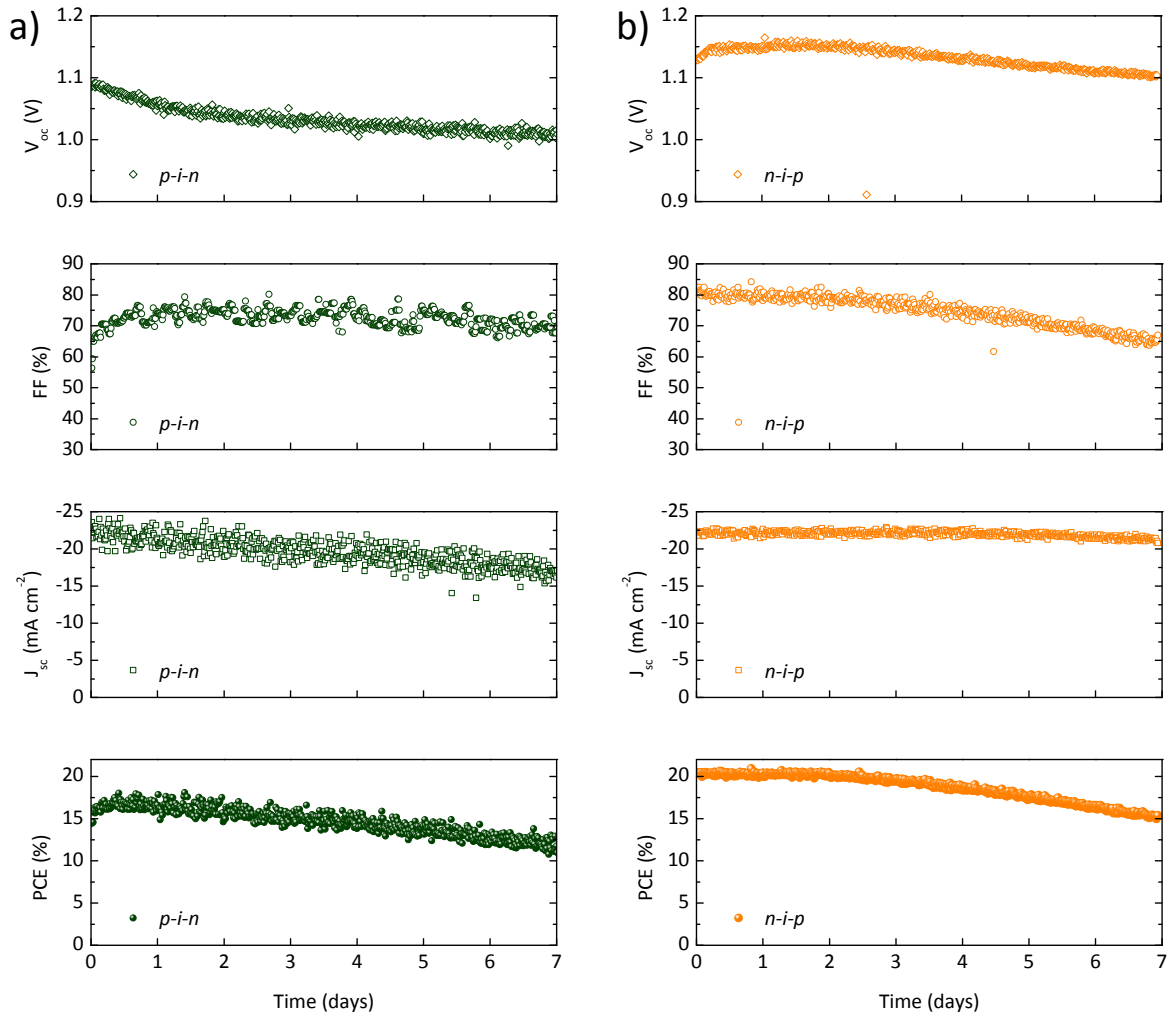

Fig. S16 Comparison of the lifetime of (a) *p-i-n* and (b) *n-i-p* perovskite devices. The photovoltaic parameters are extracted while the cells are kept under continuous illumination at short circuit conditions and with no temperature control.

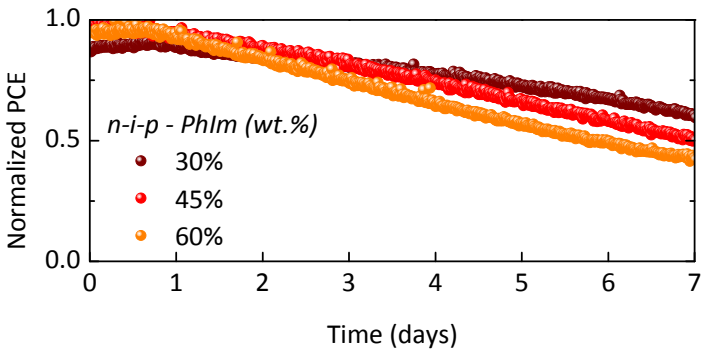

Fig. S17 Evolution of the PCE (normalized here for comparison) for a series of *n-i-p* solar cells with increasing concentration of the PhIm dopant in the n-ETL front contact.